MÜHENDİSLİK FAKÜLTESİ

Uluslararası Mühendislik Araştırma ve Geliştirme Dergisi
International Journal of Engineering Research and Development

UMAGD, (2022) 14(2), 544-551.

10.29137/umagd.1050430

Cilt/Volume:14 Sayı/Issue:2 Temmuz/July 2022

Araştırma Makalesi / Research Article

The Effect of Cu Doping On The Structural Properties and Electrical Resistivity Of $MAPbI_3$ Perovskite Thin Films

Satiye Korkmaz[1]

[1]*Department of Electrical-Electronics Engineering, Faculty of Engineering, Karabük University, 78050, Karabük, TURKEY*

***Başvuru/Received**: 29/12/2021* ***Kabul / Accepted**: 24/03/2022* ***Çevrimiçi Basım / Published Online:** 31/07/2022*

***Son Versiyon/Final Version**: 31/07/2022*

Abstract

Perovskite thin films have good power conversion efficiency because they have high carrier mobility and a long carrier lifetime. As a result of the research, the yield of perovskite materials has recently reached a maximum efficiency of 31% in the laboratory environment. To investigate the effects of doping on perovskite thin films' structural, surface, and electrical resistivity, structural properties of undoped and 10% Cu-doped perovskite thin films were characterized with XRD, FESEM, EDX, and AFM. Their electrical measurements are carried out using four-point probe method. The resistivity of undoped and 10% Cu-doped perovskite thin films decreased asymptotically with voltage increase.

Key Words

"Perovskite thin film, methylamine lead iodide, electrical resistivity"

***Corresponding Author:** satiyekorkmaz@karabuk.edu.tr*

1. Introduction

Gustav Rose discovered a mineral species with a different crystal structure in the Ural Mountains in 1839; this mineral was $CaTiO_3$. It is named "Perovskite" after the Russian mineralogist Lev Perovski, and this name is used for the structure instead of calling it mineral (Gustav, 1840). The crystal structure of perovskite, which Victor Goldschmidt first defined, is represented by the formula ABX_3, where A and B represent cations and X the anion (Goldschmidt, 1926). Structures with different properties can be created with other elements; therefore, each perovskite structure may exhibit different electrical, optical, and physical properties. Thanks to their high efficiency and low cost, they have been widely used and applied in photovoltaic devices. As shown in Figure 1, in the perovskite compound (ABX_3), A, B, and X form the 3D structure (methylammonium (MA), lead (Pb), and iodide (I), respectively). In general, it has a cubic structure and α phase, where Pb has six nearest neighbors I ions (octahedral), and MA has a twelve-fold coordination region. Of the organic-inorganic hybrid lead perovskites, methylammonium lead halides ($MAPbX_3$) (X=I, Br, Cl) are attention-grabbing with their high absorption coefficients in a wide spectral range, high charge carrier mobility, and low exciton binding energies.

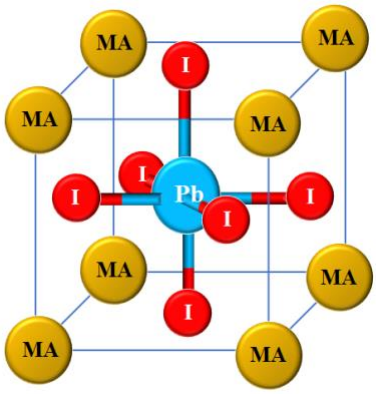

Fig. 1. Structure of $MAPbI_3$ perovskite (Soucase et al., 2016).

Perovskite films are produced using organic/inorganic materials via different methods such as spray pyrolysis, spin coating, and chemical vapor deposition (Chen et al. 2014; Barrows et al. 2014; Chen et al. 2014; Docampo et al., 2014; Leyden et al., 2014). Various techniques have been proposed, especially for the spin coating method. The most widely used method is the anti-solvent method (Jeon et al., 2014; Xiao et al., 2014; Zhou et al., 2015; Liu et al., 2015; Sun et al., 2016).

Brenner et al. investigated the relationship between the crystal structure and synthesis conditions. They concluded that the two-step method is more effective for synthesizing high-quality perovskites than one-step and multi-step perovskite film preparation methods (Brenner et al.. 2016). Burschka et al. found that in $MAPbI_3$ solar cells, the perovskite morphology formed by the reaction of PbI_2 with MAI is determined by the morphology of the first PbI_2 layer (Chen, 2017; Burschka et al., 2013; Chen et al., 2015). Perez et al. obtained perovskite films with various crystal sizes using the simple and cost-effective method they developed to produce $MAPbI_3$ thin films. They demonstrated the relationship between film morphologies, grain size, and high yield by controlling the transformation parameters (Perez et al. 2020). H.Choi et al.'s objective were to increase heterojunction hybrid solar cells' efficiency by doping cesium into $MAPbI_3$ perovskite thin films. They produced a high-performance hybrid solar cell by doping 10% cesium to the $MAPbI_3$ perovskite structure via thermal evaporation under a high vacuum (Choi et al., 2014). J. Costa et al. described a physical vapor deposition method for producing high-purity crystalline $MAPbI_3$ perovskite thin films under high vacuum conditions. Perovskite thin-film production via optimized physical vapor deposition method provided a homogeneous, stable, and pure perovskite layer. Compared to other methods, two or more components are deposited simultaneously, which offers advantages such as multilayer deposition, layer thickness control, stoichiometry control, prevention of solvents, and potentially low production costs (Costa et al., 2018).

In this study, fluorine tin oxide (FTO) substrates were coated with undoped and 10% Cu-doped perovskite films. The films' structural properties were determined by XRD, composition analysis by EDX, surface morphology by FESEM, and film thickness by AFM analysis. Electrical resistivity measurements were performed using the four-point probe method, with a Keithley 2400 sourcemeter and 2100/220 Keithley multimeter.

2. Experimental

2.1. Preparation of Perovskite thin films

Two FTO (fluorine tin oxide) substrates of 70 mm x 50 mm were used. The cleaning process was done appropriately and systematically. The substrates were first washed using detergent and distilled water, then rinsed with distilled water, dried in the oven, and then became ready for use. Firstly, the solution for undoped perovskite thin film was prepared: 0.316 g ($2x10^{-4}$ mole) of CH_3NH_2I and 0.922 g ($2x10^{-4}$ mole) of PbI_2 were weighted and mixed with 20 ml of DMF (dimethylformamide) and 10 ml of methanol in a beaker, forming a homogeneous solution. For 10% Cu-doped perovskite thin film, the same perovskite solution was prepared in a second beaker. 25 ml

of distilled water and 0.1208 g Cu $(NO_3)_2$ (10% Cu doping) were added to the prepared solution. Substrates were immersed into the prepared solutions, left for 1 hour, then placed in an oven at 70℃, and dried for 15 minutes.

2.2. Characterizations

X-ray patterns are examined by X-ray diffraction (XRD) with a $CuK\alpha_1$ radiation source (BRUKER AXS D8 model, λ=1.5406 Å) over the range of $10°<2\theta<50°$. 2D surface morphology of the thin films is examined by SEM (Carl Zeiss Ultra Plus Gemini FESEM); the film thickness, surface roughness, and 3D surface morphology are studied by AFM (Veeco Multimode 8). I-V measurements were taken with Keithley 2400 Sourcemeter device and 2100/220 Keithley multimeter, and resistivity of the films was calculated. I-V and ρ-V curves were obtained for each sample.

3. Results and Discussion

3.1. Structural and Surface Properties of Perovskite Thin Films

The doping process significantly affects the thin films' surface morphologies and compositions. The surface morphologies and compositions of undoped and 10% Cu-doped thin films deposited on the FTO substrate were examined, and found that they exhibit different physical properties. Figures 2 and 3 show SEM images and EDX analysis results of undoped and 10% Cu-doped thin films, respectively. Compared to the undoped perovskite thin film in Figure 2a, in Figure 3a Cu adhered very well to the surface by showing a homogeneous distribution. As can be better understood from the magnifications in Figures 3b and c, new formations were observed in the $CH_3NH_3PbI_3$ superstructure after Cu doping. Cu spheres formed a homogeneous and tight structure without agglomeration on the surface. EDX composition analyzes in Figure 2b, and Figure 3d showed the proportional distribution of Cu within the structure.

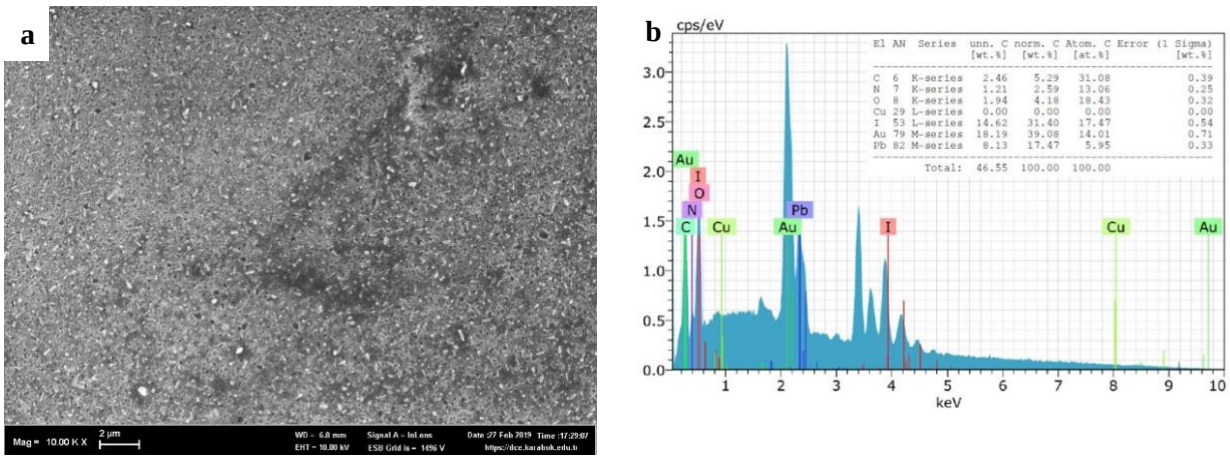

Fig. 2. Undoped perovskite thin films **(a)** SEM image **(b)** EDX analysis.

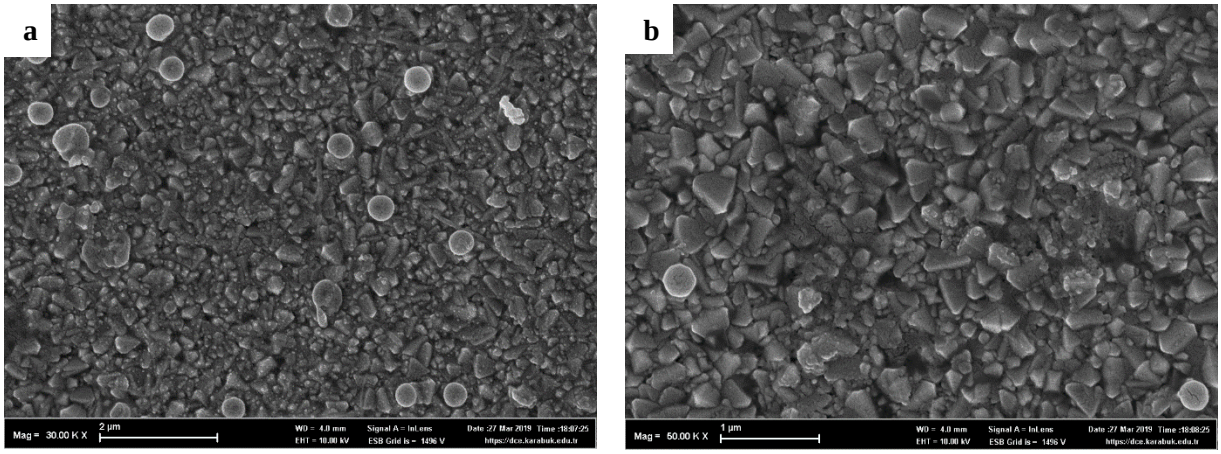

Fig. 3. 10% Cu-doped perovskite thin films **(a,b,c)** SEM images **(d)** EDX analysis.

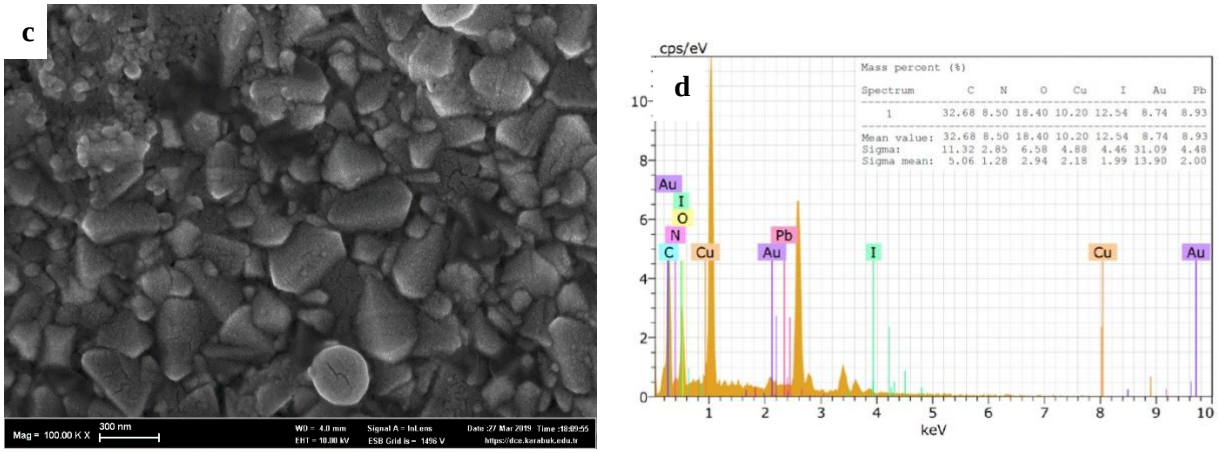

Fig. 3 ***(cont.)***. 10% Cu-doped perovskite thin films **(a,b,c)** SEM images **(d)** EDX analysis.

The structural properties of the thin films deposited on FTO were determined using XRD patterns. Figure 4 shows their XRD patterns. In the XRD diffraction patterns of the films drawn in the 2θ=10°-50° range, the diffraction peaks of undoped and 10% Cu-doped perovskite thin films at 2θ=12.64° and 26.32° are associated with the hexagonal crystal structure of PbI_2 (Filho& Marques, 2018). As can be seen from Figure 4, the 2θ diffraction peaks of $MAPbI_3$ at 14.08º (110), 28.5° (220), 32° (310) confirm the complete formation of $MAPbI_3$ (Chiang et al., 2014; Im et al., 2011). A preferred growth orientation along the (110) direction was observed in the XRD pattern of $MAPbI_3$ film, along with corresponding peaks in other directions. The peaks correspond to the pure tetragonal (β) phase of the $MAPbI_3$ perovskite (Guo et al., 2016; Zhou et al., 2015). The diffraction peaks of $MAPbI_3$ around 2θ=14°, 28°, and 32.4°, which are apparent in the undoped perovskite thin film, disappeared in the 10% Cu-doped perovskite thin film (Basumatary&Agarwal, 2020).

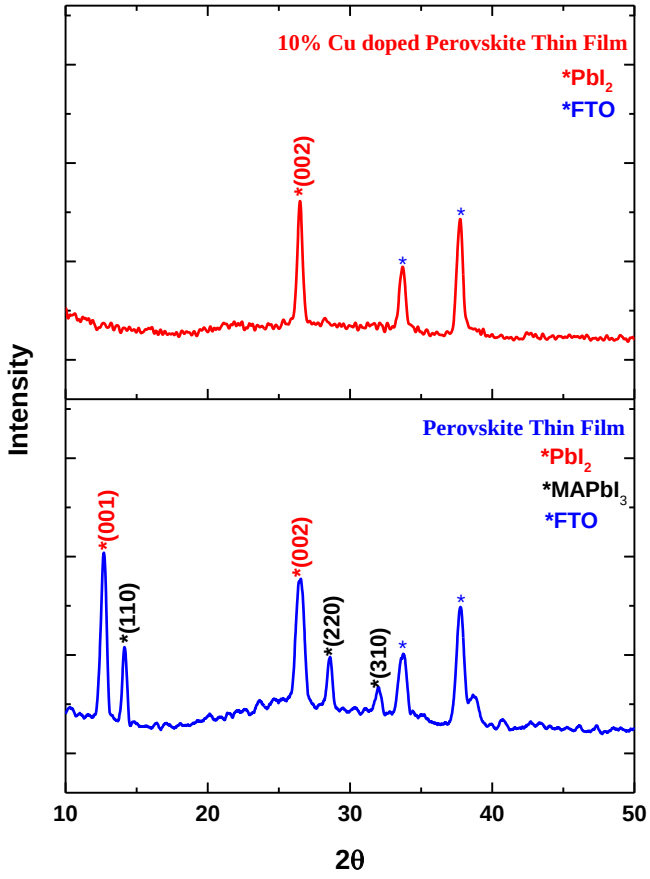

Fig. 4. XRD analysis of undoped and 10% Cu-doped perovskite thin films.

AFM analyzes are performed to determine 3D surface morphologies and surface roughness of undoped and 10% Cu-doped thin films; the results are shown in Figure 5. The surface roughness/coarseness was 236.01 nm and 114.11 nm for undoped (Figure 5a,b) and 10% Cu-doped (Figure 5c,d) perovskite thin films. 10% Cu-doped perovskite thin films' surface roughness/coarseness is lower because the crystallites are spherical and have a uniform distribution. The surface becomes more homogeneous and consists of densely packed grains.

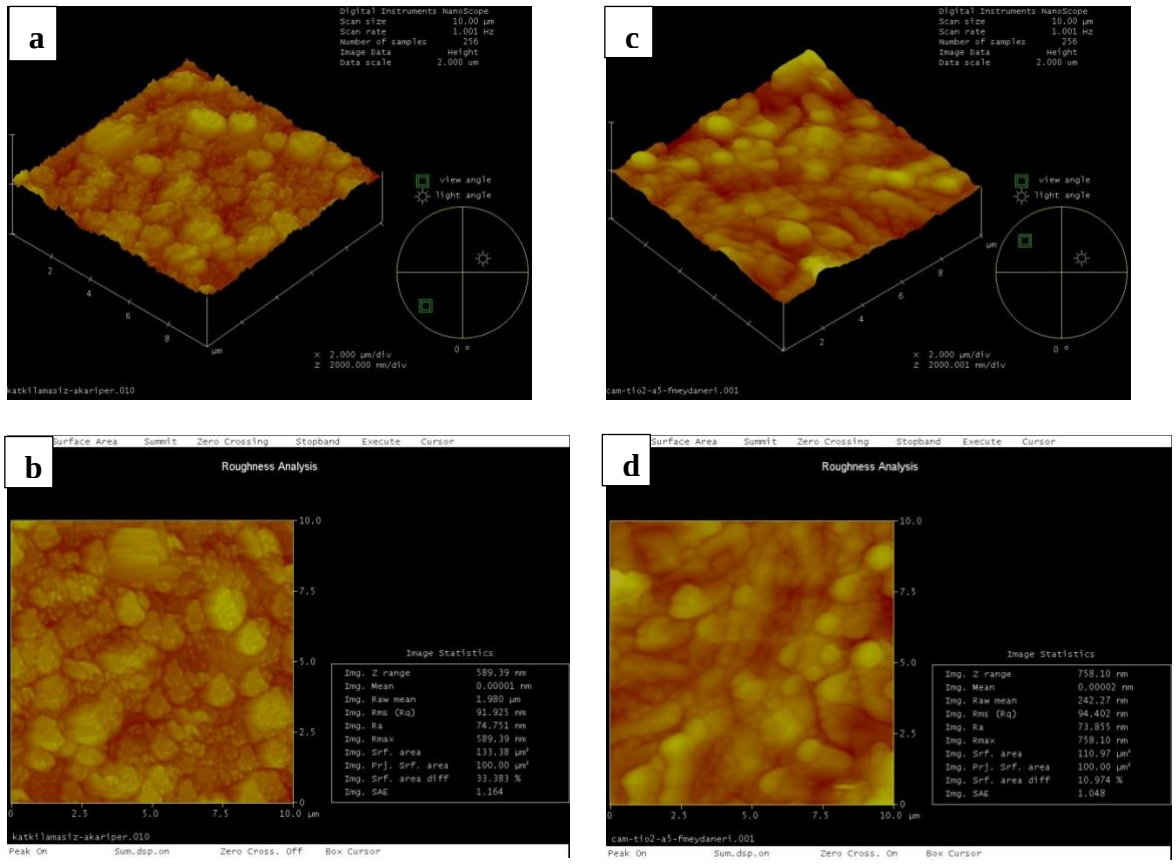

Fig. 5. AFM images (**a,b)** Undoped perovskite thin films (**c,d)** 10% Cu-doped perovskite thin films.

3.2. Electrical Resistivity Measurements

The electrical resistivity of undoped and 10% Cu-doped perovskite thin films was measured with the Keithley 2400 sourcemeter and 2100/220 Keithley multimeter using the four-point probe method. The probes' radius was 0.5 mm, and the distance between them was 1 mm. The contacts were made on the film surface with a silver paste (Ag), then the probes gently/softly touched them. All measurements were made at room temperature and in the dark.

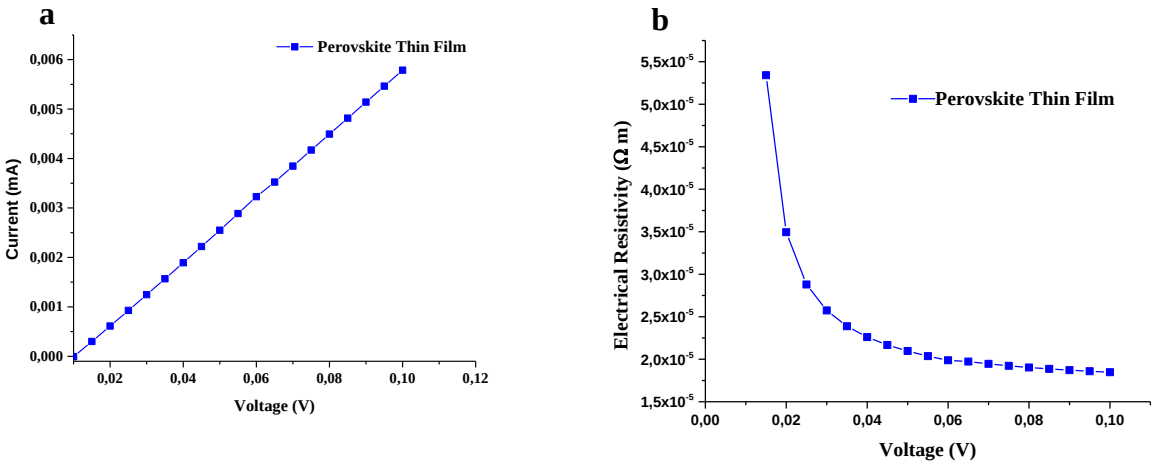

Fig. 6. I-V and ρ-V curves of Undoped Perovskite Thin Films.

I-V values of the films were taken, and resistivities were computed using Equation (I). The thin films ' I-V and ρ-V curves are shown in Fig. 6 and Fig.7. The resistivity was calculated for both thin films with the following equation (Tezel et al., 2019; Tezel et al., 2019; Tezel et al., 2021).

$$\rho = \frac{\pi\, t}{\ln 2}\left(\frac{V}{I}\right) \quad \text{(I)}$$

V, I, and t represent voltage, current, and film thickness. Accordingly, undoped and 10% Cu-doped perovskite thin films' electrical resistivities decrease asymptotically as the applied voltage increases.

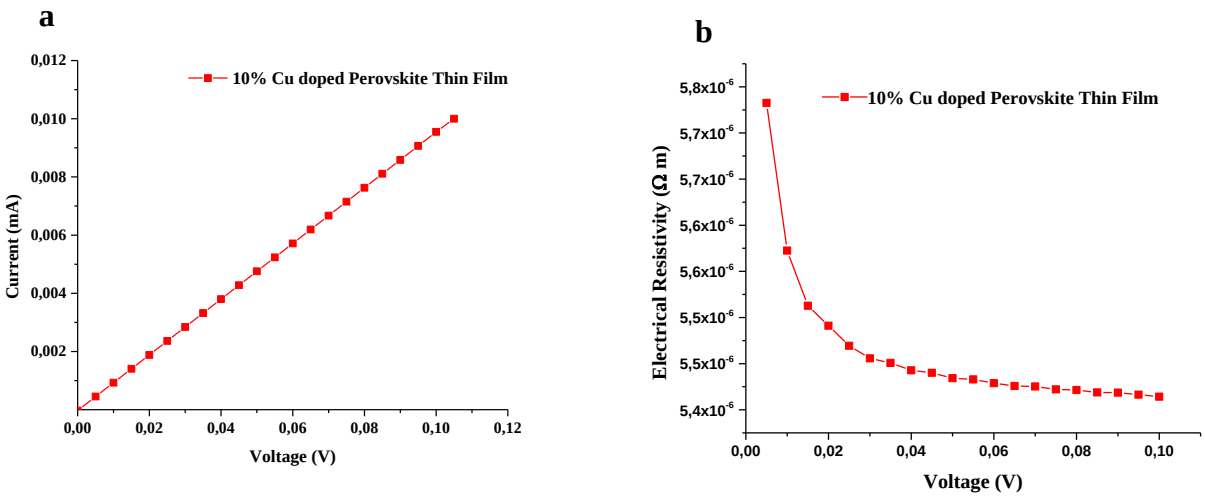

Fig. 7. I-V and ρ-V curves of 10% Cu-doped Perovskite Thin Films

4. Conclusion

Metal oxides are preferred as electron transport layers in perovskite thin films because of their thermal and chemical stability. Copper has created a promising hall transfer layer with very high thermal and electrical conductivity in thin-film technology. It does not show any signs of deterioration and does not lose its stability when stored in atmospheric conditions. In this study, undoped and 10% Cu-doped perovskite thin films were produced on FTO. Their structural characterizations were carried out with XRD, FESEM, EDX, and AFM, and the effects of doping were examined. Electrical resistivity values for Undoped and 10% Cu-doped perovskite thin films were determined as 2.36×10^{-5} Ωm and 5.46×10^{-6} Ωm, respectively. These effects show that introducing Cu doping to perovskit thin films changes the electrical properties of the material significantly. Cu additives had a reducing effect on the crystallization in the thin film. When undoped and 10% Cu-doped perovskite thin films were compared in SEM images, the homogeneous and densely packed grains in 10% Cu-doped perovskite thin films reduced the resistivity. According to literature, flat crystalline structures don't form spaces. If there are gaps between the particles, the resistance increases. This explains why the resistance in our study was lower than the literature (Targhi et al., 2018; Basumatary & Agarwal, 2019). The use of Cu as a dopant is an effective method of improving the electrical resistivity of perovskit thin films for device applications. As a way forward and due to prominent conductive nature of the synthesized material, it could be suitable alternative material for multiple applications like solar cell and energy storage.

Declaration of Competing Interest

The author declares that they have no known competing financial interests or personal relationships that could have influenced the work reported in this paper.

Referanslar

Barrows, A. T., Pearson, A. J., Kwak, C. K., Dunbar, A. D. F., Buckley, A. R., Lidzey, D. G. (2014). Efficient Planar Heterojunction Mixed-Halide Perovskite Solar Cells Deposited via Spray-Deposition, Energy Environ. Sci. 7, 2944–2950. doi:10.1039/C4EE01546K.

Basumatary, P., Agarwal, P. (2019). Two-step fabrication of MAPbI3 perovskite thin films with improved stability, Bull. Mater. Sci. 42, 268. doi:10.1007/s12034-019-1959-1.

Basumatary, P., Agarwal, P. (2020). Photocurrent transient measurements in $MAPbI_3$ thin flms, Journal of Materials Science: Materials in Electronics, 31, 10047–10054. doi:10.1007/s10854-020-03549-7.

Brenner, T.M., Rakita, Y., Orr, Y., Klein, E., Feldman, I., Elbaum, M., Cahen, D., Hodes, G. (2016). Conversion of single crystalline PbI2 to CH3NH3PbI3: Structural relations and transformation dynamics, Chem. Mater., 28, 6501–6510. doi:10.1021/acs.chemmater.6b01747.

Burschka, J., Pellet, N., Moon, S.-J., Humphry-Baker, R., Gao, P., Nazeeruddin, M.K., Grätzel, M. (2013), Sequential deposition as a route to high-performance perovskite-sensitized solar cells, Nature 499 316–320. doi:10.1038/nature12340.

Chen, C. -W., Kang, H. -W., Hsiao, S. -Y., Yang, P. -F., Chiang, K. -M., Lin, H. -W. (2014). Efficient and Uniform Planar-Type Perovskite Solar Cells by Simple Sequential Vacuum Deposition, Adv. Mater. 26, 6647–6652. doi: 10.1002/adma.201402461.

Chen, H. (2017). Two-Step Sequential Deposition of Organometal Halide Perovskite for Photovoltaic Application, Adv. Funct. Mater., 27, 1–19. doi: 10.1002/adfm.201605654.

Chen, H., Wei, Z., Zheng, X., Yang, S. (2015). A scalable electrodeposition route to the lowcost, versatile and controllable fabrication of perovskite solar cells, Nano Energy, 15, 216–226. doi:10.1016/j.nanoen.2015.04.025.

Chen, Q., Zhou, H., Hong, Z., Luo, S., Duan, H. -S., Wang, H. -H., Liu, Y., Li, G., Yang, Y. (2014). Planar Heterojunction Perovskite Solar Cells Via Vapor-Assisted Solution Process, J. Am. Chem. Soc. 136, 622–625. doi:10.1021/ja411509g.

Chiang, C.-H., Tseng, Z.-L., Wu, C.-G. (2014). Planar heterojunction perovskite/PC71BM solar cells with enhanced open-circuit voltage via a (2/1)-step spin-coating process, J. Mater. Chem. A, 2, 15897–15903. doi:10.1039/c4ta03674c.

Choi, H., Jeong, J., Kim, H., Kim, S., Walker, B., Kim, G., Kim, J.Y. (2014). Cesium doped methylammonium lead iodide perovskite light absorber for hybrid solar cells, Nano Energy, 7 80-85. doi:10.1016/j.nanoen.2014.04.017.

Costa, J.C.S., Azevedo, J., Araujo, J.P., Santos, L.M.N.B.F., Mendes, A. (2018). High purity and crystalline thin films of methylammonium lead iodide perovskites by a vapor deposition approach, Thin Solid Films, 664, 12-18. doi:10.1016/j.tsf.2018.08.026.

Docampo, P., Hanusch, F. C., Stranks, S. D., Döblinger, M., Feckl, J. M., Ehrensperger, M., Minar, N. K., Johnston, M. B., Snaith, H. J., Bein, T. (2014). Solution Deposition-Conversion for Planar Heterojunction Mixed Halide Perovskite Solar Cells, Adv. Energy Mater. 4, 1400355. doi: 10.1002/aenm.201400355.

Filho, J. M. C. S. and Marques, F. C. (2018), Growth of Perovskite Nanorods from PbS Quantum Dots, Energy and Sustainability, 3, 1843-1848. doi: 10.1557/adv.2018.188.

Goldschmidt, V. M. (1926). Die Gesetze Der Krystallochemie, Die Naturwissenschaften, 14 477–485. doi: 0.1007/BF01507527.

Guo, X., McCleese, C., Kolodziej, C., Samia, A.C., Zhao, Y., Burda, C. (2016). Identification and characterization of the intermediate phase in hybrid organic–inorganic $MAPbI_3$ perovskite, Dalton Trans., 45, 3806–3813. doi: 10.1039/c5dt04420k.

Gustav, R. (1840). Beschreibung Einiger Neuen Mineralien Des Urals, Annalen Der Physik, 126(8) 652–56, doi: 10.1002/andp.18401260807.

Im, J.-H., Lee, C.-R., Lee, J.-W., Park, S.-W., Park, N.-G. (2011). 6.5% efficient perovskite quantum-dot-sensitized solar cell, Nanoscale, 3, 4088–4093. doi: 10.1039/c1nr10867k.

Jeon, N. J., Noh, J. H., Kim, Y. C., Yang, W. S., Ryu, S. (2014). Seok, S., Solvent Engineering for High-Performance Inorganic-Organic Hybrid Perovskite Solar Cells, Nat. Mater. 13, 897–903. doı: 10.1038/nmat4014.

Jeon, N.J., Noh, J.H., Kim, Y.C., Yang, W.S., Ryu, S., Il Seol, S. (2014). Solvent engineering for high-performance inorganic-organic hybrid perovskite solar cells, Nat. Mater. 13 897–903. doi:10.1038/nmat4014.

Leyden, M. R., Ono, L. K., Raga, S. R., Kato, Y., Wang, S., Qi, Y. (2014). High Performance Perovskite Solar Cells by Hybrid Chemical Vapor Deposition, J. Mater. Chem. A 2, 18742-18745. doi:10.1039/c4ta04385e

Liu, J., Gao, C., He, X.L., Ye, Q.Y., Ouyang, L.Q., Zhuang, D.M., Liao, C., Mei, J., Lau, W.M. (2015). Improved crystallization of perovskite films by optimized solvent annealing for high efficiency solar cell, Acs Appl. Mater. Inter., 7, 24008–24015. doi: 10.1021/acsami.5b06780.

Perez, M., Peled, S. S., Templeman, T., Osherov, A., Bulovic, V., Katz, E. A., Golan, Y. (2020). A Two-Step All Solution Process for Conversion of Lead Sulfide to Methylammonium Lead Iodide Perovskite Thin Films, Thin Solid Films, 714, 138367. doi: 10.1016/j.tsf.2020.138367.

Soucase, B. M., Pradas, I. G., Adhikari, K. R. (2016). Numerical Simulations on Perovskite Photovoltaic Devices, Perovskite Materials -Synthesis, Characterisation, Properties, and Applications, Dr. Likun Pan (Ed.), InTech.

Sun, X., Zhang, C.F., Chang, J.J., Yang, H.F., Xi, H., Lu, G., Chen, D.Z., Lin, Z.H., Lu, X.L., Zhang, J.C., Hao, Y. (2016). Mixed-solvent-vapor annealing of perovskite for photovoltaic device efficiency enhancement, Nano Energy, 28, 417–425. doi: 10.1016/j.nanoen.2016.08.055.

Targhi, F. F., Jalili, Y. S., Kanjouri, F. (2018). MAPbI3 and FAPbI3 perovskites as solar cells: Case study on structural, electrical and optical properties, Results in Physics, 10, 616-627. doi:10.1016/j.rinp.2018.07.007.

Tezel, N. S., Tezel, F. M., Kariper, İ. A. (2019). Surface and Electro-Optical Properties of Amorphous Sb2S3 Thin Films, Applied Physics A: Materials Science & Processing, 125, 198-214. doi:10.1007/s00339-019-2475-2.

Tezel, N. S., Tezel, F. M., Kariper, İ. A. (2019). The Impact of pH on the Structural, Surface, Electrical and Optical Properties of Nanostructured PbSe Thin Films, Materials Research Express, 6, 076422. doi:10.1088/2053-1591/ab1675.

Tezel, N. S., Tezel, F. M., Kariper, İ. A. (2021). Effects of pH on the Optical, Structural and Supercapacitive Properties of BiTe Thin Films Produced via CBD, Bulletin of Materials Science, 44, 150. doi:10.1007/s12034-021-02398-2.

Xiao, M.D., Huang, F.Z., Huang, W.C., Dkhissi, Y., Zhu, Y., Etheridge, J., Gray-Weale, A., Bach, U., Cheng, Y.B., Spiccia, L. (2014). A fast deposition-crystallization procedure for highly efficient lead iodide perovskite thin-film solar cells, Angew Chem. Int. Edit. 53, 9898–9903. doi: 10.1002/anie.201405334.

Zhou, Y., Yang, M., Vasiliev, A.L., Garces, H.F., Zhao, Y., Wang, D., Pang, S., Zhu, K., Padture, N.P. (2015). Growth control of compact $CH_3NH_3PbI_3$ thin films *via* enhanced solid-state precursor reaction for efficient planar perovskite solar cells, J. Mater. Chem. A, 3, 9249– 9256. doi:10.1039/c4ta07036d.

Zhou, Y.Y., Yang, M.J., Wu, W.W., Vasiliev, A.L., Zhu, K., Padture, N.P. (2015). Room-temperature crystallization of hybrid-perovskite thin films via solvent-solvent extraction for high-performance solar cells, J. Mater. Chem. A, 3, 8178–8184. doi: 10.1039/c5ta00477b.